

Transition metals: *d*-band hybridization, electronegativities and structural stability of intermetallic compounds

R. E. Watson

Brookhaven National Laboratory, Upton, New York 11973

L. H. Bennett

National Measurement Laboratory, National Bureau of Standards, Washington, D. C. 20234

(Received 21 August 1978)

An electronegativity scale is derived for the noble and transition metals, based on their electron-band theory description. The tendency of *d*-band electron and hole states to hybridize is used to estimate the propensity for a particular metal to gain or lose *d*-electron count and this, in turn, is used to provide the basis of the electronegativity scale. Overall agreement of this scale with Miedema's and Pauling's electronegativity is remarkably good, granted the widely divergent bases of the three scales. The results, combined with an average electron vacancy count, are then used in structural maps of transition-metal-transition-metal alloy systems.

I. INTRODUCTION

The propensity of an atom in an alloy or compound to compete with other atomic species for valence-electron charge is generally encompassed in an "electronegativity" factor. Charging effects are important to the energetics of compound formation, of course, and electronegativity scales tend to play prominent roles in our understanding of such matters as alloy solubility,¹⁻⁵ as well as in estimates, such as Miedema's, of the heats of formation of compounds.⁶ Electronegativity scales have been derived from a variety of sources: from free-atom ionization energies and electron affinities,⁷⁻⁹ from work functions,⁶⁻¹⁰ and from thermochemical data,¹¹ to name a few of the most popular. The extent to which such diversely based scales agree is remarkable, although there are differences in detail that are of quantitative significance. To date, there has been no "first principles" estimate of the electronegativity scale for the *transition* metals based on their *d*-band properties, and the main purpose of this paper is to provide such an estimate. Comparison will be made with other electronegativity scales, and the present results will then be employed in structural maps for transition-metal-transition-metal compounds.

Simons, St. John, and Bloch⁸ developed an orbital picture of the electronegativity of *nontransition* elements where *s* and *p* valence electrons act cooperatively in bonding. The change in the *s*- and *p*-electron count at an atomic site, sometimes termed charge transfer, tends to be in the same direction. The situation is quite different for transition metals, where *d* and non-*d* charge transfer are in opposite directions. In Au alloys,

for example, the Mössbauer isomer shift indicates¹² substantial *s*-like charge increases at the Au sites, whereas energy shifts in Au core levels and in the position of the Au 5*d* band are to lower energy, characteristic of the depletion of valence charge at an atomic site. This was shown¹³ to be understandable in terms of *d*-electron decreases and non-*d*-electron increases at the Au site. From this and other work, a picture is gradually emerging where the net charge change at a transition-metal site tends to be opposite in sign to that of the *d* alone.

The essential feature of a transition metal is that there are ten electron or hole *d*-band states within but a few eV of the Fermi levels ϵ_F . Hybridization of a transition metal's occupied states with the unoccupied levels of some other constituent's atom in an alloy leads to a loss of *d* weight in these occupied states and hence a loss of *d* count at the site. On the other hand, hybridization of the metal's hole states with the occupied levels of the other site leads to some occupation of these hole states, and hence an increase of *d* count. In an almost empty *d*-band metal, such as Sc or Y, the large preponderance of hole states implies a tendency to gain *d* character upon alloying, while Au and Ni with their filled, or almost filled, *d* bands can only lose. This change of charge is opposite to the general observation that Au and Ni are electronegative (i.e., they attract electron charge), whereas Sc and Y are electropositive. Now, this reverse behavior is what is required, for, as we have noted above, *d* charge does change in the "wrong" direction. Recently, we have inspected¹⁴ the body of available Mössbauer isomer-shift data for transition-metal impurities, and concluded that the

ratio of d to non- d charge transfer is, in first approximation, constant. Under the assumption that a propensity Λ for a particular d -band metal to gain d charge can be defined and estimated, this constancy leads to the establishment of an electronegativity scale $\phi = -A\Lambda$, where A is a positive constant. The ratio of d to total charge transfer may not be strictly constant across the transition-metal series, but if we assume that it varies smoothly, we obtain

$$\phi = -A\Lambda + B. \quad (1)$$

A and B will be chosen to bring our ϕ values into overall register with Pauling's electronegativity scale,¹¹ thus allowing comparison between scales.

The quantity Λ will be defined in terms of the hybridization of a particular metal's band structure with a test atom having occupied levels an energy δ below the Fermi level, and holes in the same energy distance above. The essential inputs to the calculation are a d -band density of states, the d -band width, the position of the Fermi level in the density of states, and the strength of the hybridization matrix element appropriate to a given transition metal. The first three of these factors determine the number of occupied versus hole states and their availability, energetically, for mixing. Our results are insensitive to the choice of the test-atom's level splitting δ , provided δ is not chosen too small. Details of the calculation are given in Sec. II.

The resulting electronegativity scale is shown in Fig. 1 to rise more or less smoothly across a transition-metal row, and drop on continuing to the noble metal. This drop is consistent with the ϕ of Gordy and Thomas,¹⁰ and more recently of Miedema,⁶ both of which are based on work functions. The drop is not seen in Pauling's scale for Cu and Au, whose ϕ are larger than those of their neighbors, Ni and Pt, respectively. This and other matters are considered when the present ϕ scale is compared with other scales in Sec. III. The calculations of Sec. III are for paramagnetic metals, but the discussion in Sec. IV shows that the effect on ϕ of the ferromagnetism of Fe, Co, and Ni is slight.

The present ϕ values are used in structural maps of transition-metal-transition-metal compounds in Sec. V. The purpose of such maps is to correlate the structure into which an alloy or compound forms with such factors as the difference in electronegativity of the constituents. Such mapping was introduced by St. John and Bloch⁸ for non-transition-metal compounds, and extended with considerable success by Phillips and co-

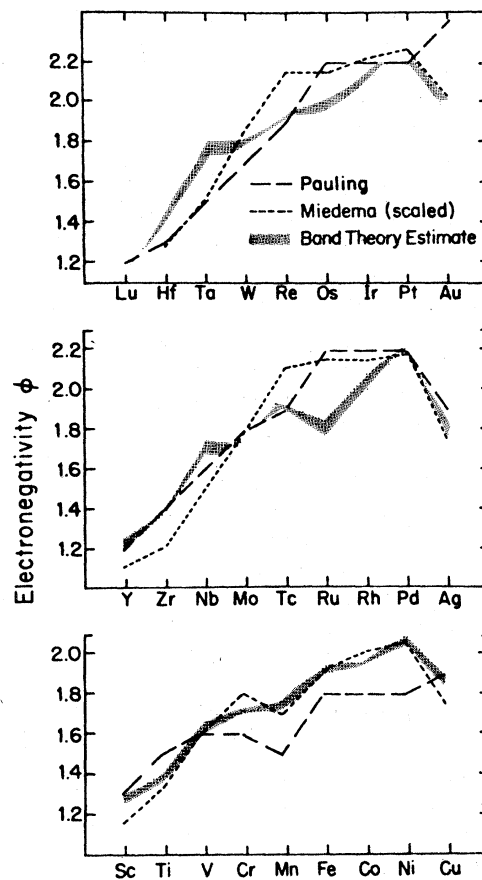


FIG. 1. Electronegativity values, derived from Eq. (1) using band theory for the transition metals. The spread is related to the choice of the level splitting δ of the test atom. Also shown is the Pauling electronegativities (Ref. 11) and a scaled version of the Miedema (Ref. 6) electronegativities.

workers.^{15, 16} St. John and Bloch defined effective valence-electron radii based on free-ion spectroscopic data, and derived an electronegativity from these. As a second parameter in their structural maps, they took the difference in the s and p electron radii, S , to provide a subtle measure of the tendency for s vs p electron bonding. The present authors considered the implications of applying a Mulliken type of electronegativity scale, based on free-atom ionization energies, to mapping of the type used by St. John and Bloch. Using ionization energies rather than radii, the S factor became a type of s - p promotion energy. The resulting scales were applied⁹ to maps of the non-transition-element compounds and to compounds

formed between transition and nontransition elements, as well. In this latter case, the second parameter was the *S* factor of the nontransition element alone. The situation for transition-metal alloys of concern to us here is quite different from that of non-transition-element compounds, since *d* and non-*d* bonding effects involve opposing charge transfer. Rather than some *s-d* analog of the *S* factor, the maps of Sec. V employ the average number of *d*-band vacancies per constituent atom in the compound as a second parameter. Reasonable success is attained.

In summary, the present investigation might be said to take the opposite tack to what is usually done. It is common to define an electronegativity scale in some way and to derive charge transfer effects in terms of the scale. It is our intent, instead, to calculate *d*-electron charge transfer and to derive an electronegativity scale in terms of this. The resulting scale will be compared with Pauling's and Miedema's scales, and then used in structural mapping.

II. THE CALCULATION OF Λ

Consider an occupied electron level ϵ_e hybridized with a set of hole states with energy ϵ_h , above ϵ_F . If the levels are orthogonal, the weight of hole character admixed into the level is, in lowest order,

$$\sum_h \frac{\gamma^2}{(\epsilon_e - \epsilon_h)^2}, \quad (2)$$

where γ is a hybridization matrix element.¹⁷ A similar expression holds for the loss of orbital character associated with a set of levels below ϵ_F admixed with a hole.

If the *d* bands of a transition metal are to hybridize with a test atom with electron levels δ below, and hole levels δ above ϵ_F , the resulting gain or loss of *d*-band character is

$$\Lambda \equiv \gamma^2 \int \left(\frac{\epsilon_i - \epsilon_F}{|\epsilon_i - \epsilon_F|} \right) \frac{\rho(\epsilon_i)}{(|\epsilon_i - \epsilon_F| + \delta)^2} d\epsilon_i, \quad (3)$$

where we have assumed a constant matrix element γ , and $\rho(\epsilon)$ is the density of states of the *d* bands. The large parenthesis inside the integral contributes the minus sign associated with the admixture of *d*-band states below ϵ_F and a plus sign for hole states above. In practice, we have replaced the integral by a sum over a density-of-states histogram. To do this, we have marked the top of *d*-band structure by a level, such as the X_5 state in the nonrelativistic fcc structure, and divided the states below into ten bins, each

containing one electron state per atom. In general, there are additional "conduction band" levels below this histogram; these levels are omitted from the sum. The integral becomes a sum over the centers of gravity of the ten bins, except for the bin in which ϵ_F falls. This bin is divided in two, the centers of gravity of its hole and electron components determined, and their contributions added to the sum to give the propensity for the addition of *d* charge

$$\Lambda = \gamma^2 \sum \left(\frac{\epsilon_i - \epsilon_F}{|\epsilon_i - \epsilon_F|} \right) \frac{W}{(|\epsilon_i - \epsilon_F| + \delta)^2}, \quad (4)$$

where the weight *W* is 1.0, except for this part of hole and electron components. This procedure suffices, provided δ does not take on too small a value. Lacking a complete set of suitable summed densities of states, we have taken those available in the literature and scaled a histogram for the appropriate structure by the bandwidth appropriate to the metal in question. The histograms and their centers of gravity are readily determined if the sum of the density of states up to some energy ϵ is tabulated as a function of ϵ , up to the top of the *d* bands. Such cases were used here. The structures for which calculations were done and the bandwidths Δ are listed in Table I: footnotes indicate the band calculation¹⁸ whose $\rho(\epsilon)$ was used in any particular case. Bandwidths were chosen by inspection of the body of calculations available in the literature.

Fermi-level positions were determined by first estimating the number of states per atom, *N*, residing in bands below the *d*-band top. Subtracting the total number of valence electrons from *N* determines the number of hole states, and hence the Fermi level. The experimental *d*-band hole counts were used to determine *N* for Ni, Pd, and Pt, and the body of band-theory results were used to extrapolate to the lighter metals. Calculations were done for Cu, Ag, and Au taking the top of their *d* bands to be 0.14, 0.29, and 0.18 Ry below ϵ_F , respectively. In general, since γ as well as $\epsilon_i - \epsilon_F$ is proportional to Δ , the detailed choice of *N* and the bandwidth are not important to the results, providing they vary slowly across a transition-metal row, as they are known to do.

The hybridization integral was obtained following Heine's derivation¹⁹ of *d*-band widths. He developed a Korringa-Kohn-Rostoker (KKR) description, where *d* orbitals on different sites interacted via hybridization with muffin-tin states. A single-site hybridization parameter

$$\gamma = \int \phi_d(r) V_d(r) j_2(Kr) r^2 dr \quad (5)$$

TABLE I. Structures, electron-energy-band parameters, and electronegativities for transition metals.

	Structures			Bandwidth Δ (Ry)	States below top of d bands, N	γ^2	ϕ ($\delta = 0.3$)
	fcc	bcc	hcp				
Sc		a	b	0.43	11.25	0.080	1.26
Ti		a	b	0.53	11.0	0.099	1.38
V		a		0.58	10.85	0.100	1.62
Cr		a		0.61	10.7	0.099	1.69
Mn	c	a		0.45	10.55	0.067	1.74
Fe	c	a		0.44	10.4	0.057	1.93
Co	c		b	0.38	10.5	0.050	1.95
Ni	c			0.34	10.6	0.046	2.09
Cu	c			0.25	...	0.036	1.88
Y			b	0.50	10.8	0.110	1.21
Zr		d	b	0.60	10.75	0.121	1.37
Nb		d		0.69	10.7	0.130	1.69
Mo		d		0.72	10.7	0.129	1.73
Tc			b	0.69	10.5	0.117	1.92
Ru			b	0.63	10.35	0.095	1.85
Rh	e			0.54	10.4	0.080	2.07
Pd	e			0.41	10.36	0.061	2.22
Ag	e			0.26	...	0.044	1.84
(La)					(11)		(est 1.05)
Lu		f	g	0.52	10.95	0.108	1.15
Hf		f	g	0.62	10.85	0.120	1.40
Ta		f		0.75	10.8	0.136	1.74
W		f		0.77	10.75	0.137	1.80
Re			h	0.74	10.65	0.130	1.95
Os			h	0.66	10.45	0.108	1.98
Ir	i			0.60	10.5	0.099	2.12
Pt	i			0.53	10.43	0.084	2.28
Au	i			0.41	...	0.071	1.97

^a bcc Fe (Wood's band results as reported by Mattheiss, Ref. 18).

^b hcp Zr (Jepson *et al.*, Ref. 18).

^c fcc Ni (self-consistent-field result, unpublished).

^d bcc Nb (Mattheiss, Ref. 18).

^e fcc Pd (self-consistent-field result, unpublished).

^f bcc Ta (relativistic calculation - Mattheiss, Ref. 18).

^g hcp Hf (Jepson *et al.*, Ref. 18).

^h hcp Re (relativistic calculation of Mattheiss, Ref. 18).

ⁱ fcc Au (relativistic linear-combination-of-atomic-orbitals fit to Christensen's results, Ref. 18).

was defined, where ϕ_d is a radial d orbital localized on a single site, V_d is the d -electron potential, and j_2 is a spherical Bessel function associated with a muffin-tin plane wave whose K equals the square root of the difference in energy between the center of gravity of the d bands and the bottom of the continuum. By making boundary-value arguments, γ was related to the bandwidth Δ by

$$\Delta = K\gamma^2 \left(\frac{n'_2(KR)}{j'_2(KR)} - \frac{n_2(KR)}{j_2(KR)} \right), \quad (6)$$

where n' and j' are derivatives of these Bessel functions and R is the muffin-tin radius. Hodges *et al.* have shown²⁰ that this prescription accurately reproduces computed d bandwidths. We have

assumed that Eq. (5) also controls the variation in the hybridization matrix between our test atoms and a transition metal, and thus γ^2 has been obtained with Eq. (6) for the bandwidths tabulated in Table I. The resulting γ^2 values are also listed in Table I so as to allow the interested reader to ascertain their contribution to the electronegativity results.

Equation (4) was evaluated for δ values of 0.1, 0.2, 0.3, and 0.4 Ry. The $\delta=0.1$ results are discernably noisy due to the coarseness of the histogram sum and the crudity in reading off the density-of-states information. For any given δ , the values of Λ for a metal taken in several structures were averaged, and the A and B of Eq. (1) obtained by linear regression with the Pauling

electronegativity scale. The results for $\delta=0.3$ are listed in Table I. The range of ϕ obtained for $\delta=0.2-0.4$ are indicated by the shaded regions in Fig. 1.

III. ELECTRONEGATIVITY RESULTS

Inspection of Fig. 1 shows the present *d*-band charge flow estimates of the electronegativity χ rising relatively smoothly across a transition-metal row and then dropping on going to the noble metals. The spread in ϕ , obtained with different values of δ , is indicated and is seen to be small compared with the differences between the three electronegativity scales represented on the figure.

The *d* bands of the noble metals are filled, with the tops of these bands lying 0.14–0.29 Ry below ϵ_F . This increases the energy denominator of Eq. (3), causing the observed drops in ϕ . The drop is most severe for Pd–Ag, which, in large part, is due to the fact that the *d* bands of Ag lie lowest below ϵ_F . Pd is in part responsible, for it has the fewest *d*-band holes among the transition metals, enhancing the sum in Eq. (3).

While ϕ generally increases as a transition-metal row is traversed, it seen to drop for Tc → Ru and discernably levels out in a number of cases (e.g., Nb → Mo, Ta → W, and Re → Os). These smaller fluctuations are due to special features of the band structure. Consider Mattheiss's density of states¹⁸ for bcc Ta, which is traced in Fig. 2. The Fermi level for Ta lies at the upper edge of a high density-of-states peak with a density-of-states minimum just above; there are

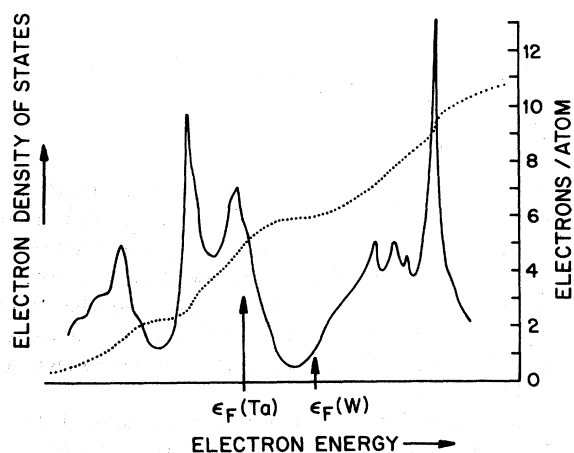


FIG. 2. Schematic tracing (solid line) of the electronic density-of-states histogram of Mattheiss for relativistic tantalum (Ref. 18). The dotted line is the integrated electron count.

many electron states, and relatively few hole states lying close to ϵ_F , the energy region important to hybridization. The ϵ_F for W lies higher in the bands, and while there is one more electron and one fewer hole per atom than for Ta, many hole states, and few electron states now lie close to ϵ_F . The increase in available electron states (and loss of holes) has been compensated by a decrease in ability for the electron states (an increase for holes) to hybridize. The flattening for Nb → Mo is due to this same feature of the body-centered-cubic $\rho(\epsilon)$. There is a similar minimum in the hcp $\rho(\epsilon)$ in the vicinity of eight electrons per atom, which is responsible for the Tc → Ru drop and the Re → Os leveling. No leveling is seen for the equivalent 3*d* pair, Mn → Fe, because neither Mn nor Fe forms in the hcp structure. The exact extent of the leveling depends on where the pair of Fermi levels fall in $\rho(\epsilon)$ and on details of how the hybridization matrix element γ varies between the pair. Inspection of the $\rho(\epsilon)$ sum alone suggests that a rise for Tc → Ru is most unlikely, though refinements in the estimates of γ may produce such a rise. The effect of broad density-of-states minima is thus to enhance the ϕ of V, Nb, Ta, Tc, and Re, while reducing those of Cr, Mo, W, Ru, and Os, respectively.

A number of the transition metals form in two crystal structures (see Table I), and our practice has been to average the Λ obtained for the two structures, since we wish to define a single ϕ value for a given element. On the whole, the results are relatively insensitive to differing structure, although in the cases of Lu and Mn the ϕ defined for one of the pair of structures differs from the average by ± 0.05 .

Let us now compare the band results with the Pauling and Miedema electronegativities displayed in Fig. 1. (We have scaled Miedema's transition- and noble-metal results by a linear regression to Pauling's so that the three sets of electronegativities are in register.) The band results do not display the plateaus seen at the upper ends of the transition-metal rows in the other scales; for example, the ϕ of Ru, Rh, and Pd are constant, or almost so, for the other scales, while having significant slope for ours. In fact, the greatest discrepancy between our and the other scales occurs for Ru. Our results are in quite good register with Miedema's for the 3*d* elements, implying that they are not as electropositive with respect to their 4*d* and 5*d* counterparts as is indicated in the Pauling scale. In general, the 4*d* ϕ of the heavier transition metals are equal to, or only slightly less than, their 5*d* counterparts, with the 3*d* lying significantly farther below. With the exception of low-lying Ru, this is true of the

present band results and involves an interplay of band filling effects and the variation in hybridization matrix elements (see the γ^2 values of Table I). The other two electronegativity scales display dips for Cr–Mn, whereas the band results show a flattening. The other band-theory flattenings, which have been discussed above, are not discernable in the Pauling and Miedema scales. The effect of these is to cause our ϕ for Ta and Nb to be high, and those for Ru and Os to be low, relative to the other two scales.

The band and Miedema ϕ for the noble metals lie lower than the ϕ of the transition metals to their left, while the Pauling values for Au and Cu do not. An experimental case can be made for either trend. In Miedema's description of the heats of formation of transition-metal alloys, a negative contribution is associated with the square of the difference in electronegativities and a positive contribution from a mismatch in valence-electron densities. As a rule, the noble metals have positive heats of formation with elements in the middle of a transition-metal row, such as W, while having negative or near-zero values upon alloying with Pd and Pt. The positive signs require small electronegativity differences, hence dips in ϕ for Cu and Au. On the other hand, Au Mössbauer isomer-shift data suggest¹² that there is always a flow of non- d charge onto Au sites when alloyed with a transition metal. These results, taken with core level shifts, as measured with photoelectron spectroscopy, suggests that the net charge transfer is always onto Au sites,^{13, 21, 22} a situation consistent with the Pauling electronegative scale. Granted the present state of our understanding, different experimental situations appear consistent with different scales. What is remarkable is the extent to which the three diversely derived scales of Fig. 1 agree.

IV. EFFECT OF FERROMAGNETISM

The calculations of Secs. II–III assumed paramagnetic band-theory descriptions where electron states of either spin are equally occupied. In the Stoner–Wohlfarth description²³ of Fe, Co, and Ni, the bands are simply exchange split with the difference in majority and minority spin subband occupations equal to the known spin magnetic moment of the ferromagnetic metal; e.g., the majority spin band of Fe having 2.2 more electron states the minority. Summing Eq. (3), we obtain changes in ϕ of 0 ± 0.02 , 0.05 ± 0.02 , and -0.01 ± 0.01 for Fe, Co, and Ni, respectively. These effects are negligible.

V. STRUCTURAL MAPS OF TRANSITION-METAL COMPOUNDS

One recent application of electronegativity scales has been to structural maps, where the structures associated with a particular class of binary compounds are related to parameters such as the difference in electronegativity of the constituents. Earlier work involved compounds with nontransition elements as one⁹ or both^{8, 9, 15, 16} components. In this section we will consider the case of transition-metal–transition-metal compounds, employing differences in the band-theory ϕ in the plots.

There remains the question of the second parameter to be used. Simons and Bloch introduced a parameter S , which provided a measure of the relative tendency for s vs p bonding. In their scheme, it was the difference in effective orbital radii; more recently, we employed the difference in s and p ionization energies. In either case, the average S value of the constituents was used for compounds involving a pair of nontransition elements. As we have already noted, the situation is different with transition-metal alloys because d and non- d charge transfer oppose one another. The analog of S , in terms of d and non- d radii or ionization energies, may be defined, but preliminary investigation suggests that such quantities are not particularly useful in structural maps.²⁴ This matter deserves further investigation, but we will make a different choice of a second parameter here.

The number of electron states in a transition metal N_e or the number of vacancies or holes in the d bands above the Fermi level N_v have proven useful parameters in the past to the metal physicist. When the Fermi level falls within the d bands, these quantities and the N of Table I are related by

$$N_v = N - N_e, \quad (7)$$

which, for noble metals, yields

$$N_v = 0 \text{ and } N_e = 11. \quad (8)$$

These quantities are not unrelated to the electronegativity (after all, Nature uses only one independent parameter, namely, the nuclear charge Z), but they do provide a different measure of the factors contributing to alloying.²⁵ We choose to use the average value of the electron vacancy count \bar{N}_v of the alloy as the second parameter in the plots. With this choice, the maps are based on a pair of parameters that are both derived from a band-theory description of the transition metals.

Structural maps for NM , NM_2 , and NM_3 compounds are given in Fig. 3. The compounds so

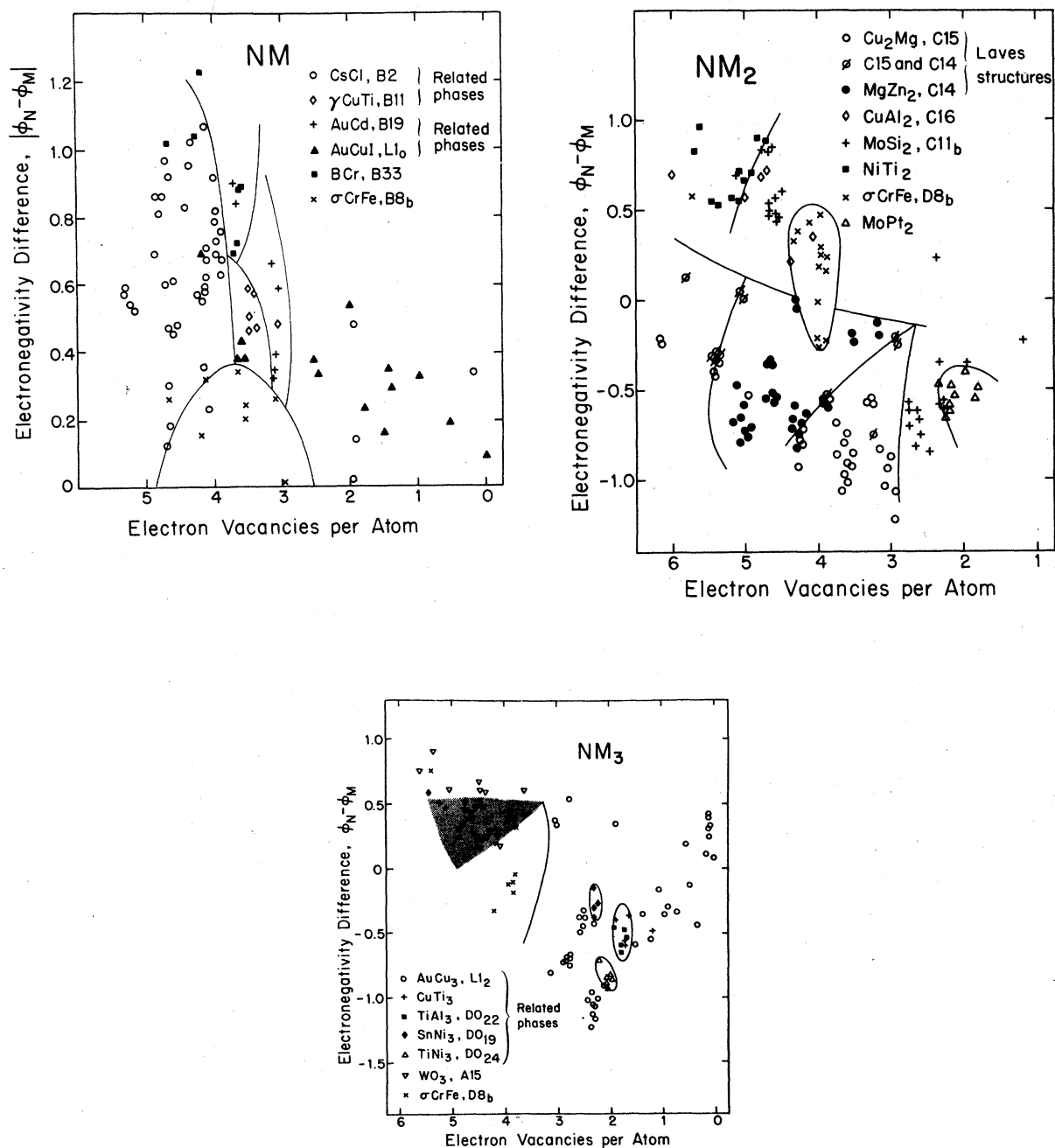


FIG. 3. Structural maps for transition-metal-transition-metal compounds, using the band-theory estimate of electronegativities and *d*-band vacancies. See Table II for compounds shown.

represented and their structures are listed in Table II. Landolt-Börnstein²⁶ has been used as the final arbiter of whether a compound does or does not form in a particular structure. $\Delta\phi$ has been taken to be positive for the equiatomic *NM* compounds and has the sign defined by

$$\Delta\phi \equiv \phi_N - \phi_M \quad (9)$$

for the *NM₂* and *NM₃* sets. As a general rule, compounds forming in a particular structure lie in or near well-defined regions on a map. Lines have been drawn to provide roughly defined

TABLE II. Compounds represented in Fig. 3.

<i>NM</i>							
BCr, B-33	AuCu L1 ₀	γ -CuTi, B-11	σ -CrFe, D8 _b	AuCd, B-19	CsCl, B-2		
HfNi	AuCu-I	AgZr	Co-Cr	IrMo	AgLa	LuPd	
HfPt	CoPt	AuHf	CoV	IrW	AgLu	LuRh	
LaNi	FePt	AuTi	CrFe	NbPt	AgSc	β -MnPd	
LaPt	FePd	γ -CuTi	FeMo	PtTi	AgY	MnV	
LaRh	IrMn	PdTa	Fe-Tc	PtV	AuLu	NiSc	
NiZr	IrNb	AgTi	FeV	MoRh	AuSc	OsTi	
PtZr	MnPt		Re-W	PdTi	AuY	OsV	
	MnRh		NbRe		CoFe	OsZr	
	NbRh				CoHf	PdSc	
	NiPt				CoSc	PtSc	
	RhTi				CoTi	ReTi	
	AuMn				CoZr	RhSc	
	FeNi				CuLu	RuSc	
	IrTa				β -Cu-Pd	RuTi	
					CuSc	Ru-V	
					CuY	RuZr	
					FeRh	TaTc	
					HfRh	TcTi	
					HfRu	TcV	
					HfTc	AuLa	
					IrLu	RhY	
					IrSc		
<i>NM₂</i>							
MgZn ₂ , C-14	C-14, C-15	MgCu ₂ , C-15	σ -CrFe, D8 _b	MoSi ₂ , C-11 _b	CuAl ₂ , C-16	MoPt ₂	NiTi ₂
MoFe ₂	TaCo ₂	HfCo ₂	OsW ₂	AgZr ₂	CoSc ₂	CrNi ₂	NiTi ₂
NbFe ₂	ZrCr ₂	LuCo ₂	OsMo ₂	HfAu ₂	CoZr ₂	MoPd ₂	PtTi ₂
TaFe ₂	NbCo ₂	ScCo ₂	MoRe ₂	AuHf ₂	NiHf ₂	MoPt ₂	CoHf ₂
TiFe ₂	HfCr ₂	TiCo ₂	RhNb ₂	LuAu ₂	NiTa ₂	NbPd ₂	CoTi ₂
WFe ₂	NbCr ₂	YCo ₂	ReZr ₂	MnAu ₂	NiZr ₂	NbPt ₂	FeHf ₂
HfMn ₂	TaCr ₂	ZrCo ₂	AuTa ₂	AuMn ₂	CoTa ₂	VNi ₂	FeTi ₂
HfOs ₂	TiCr ₂	LuFe ₂	OsCr ₂	TiAu ₂		TaPd ₂	IrHf ₂
LuMn ₂	ZrIr ₂	ZrFe ₂	RuCr ₂	AuZr ₂		VPd ₂	PtHf ₂
LuOs ₂	HfMo ₂	HfV ₂	CrTc ₂	CuHf ₂		VPt ₂	RhHf ₂
LuRe ₂	TaV ₂	HfW ₂	RhTa ₂	CuTi ₂			NiSc ₂
LuRu ₂	HfFe ₂	LaIr ₂	IrNb ₂	CuZr ₂			PdSc ₂
LuTc ₂		LuIr ₂	MoMn ₂	PdHf ₂			
NbMn ₂		ScIr ₂	NiV ₂	TaNi ₂			
TaMn ₂		YIr ₂	CrRe ₂	PdTi ₂			
TiMn ₂		LaNi ₂		ZrPd ₂			
ZrMn ₂		LaOs ₂		PdZr ₂			
ScOs ₂		LaPt ₂		AgHf ₂			
YOs ₂		LaRh ₂		LuAg ₂			
ZrOs ₂		LaRu ₂		ScAg ₂			
ScRe ₂		LuNi ₂		YAg ₂			
YRe ₂		LuRh ₂		AgTi ₂			
ZrRe ₂		YMn ₂		ScAu ₂			
ScRu ₂		ZrMo ₂		VAu ₂			
YRu ₂		ScNi ₂		YAu ₂			
ScTc ₂		YNi ₂		RhTi ₂			
YTc ₂		YPt ₂		ScCu ₂			
ZrTc ₂		YRh ₂		ZrAu ₂			
ScFe ₂		ZrV ₂					
ScMn ₂		ZrW ₂					
HfTc ₂		YFe ₂					
HfRe ₂							

TABLE II. (Continued)

NM_3		$WO_3, A-15$	$CuTi_3$	$SnNi_3, DO_{19}$	σ -CrFe, $D8_b$	$TiAl_3, DO_{22}$	$TiNi_3, DO_{24}$
LuPt ₃	LaPd ₃	AuTa ₃	AgZr ₃	WCo ₃	WTe ₃	NbPd ₃	TiNi ₃
PtAg ₃	LuPd ₃	AuNb ₃	HfAu ₃	Wrh ₃	VRe ₃	VNi ₃	HfPd ₃
AgPt ₃	MnNi ₃	AuZr ₃	ZrAu ₃	CoZr ₃	CrMn ₃	TaPd ₃	HfPt ₃
AuNi ₃	PtMn ₃	CoV ₃	CuTi ₃	MoIr ₃	IrTa ₃	VPd ₃	TiPd ₃
NiAu ₃	MnPt ₃	IrCr ₃	MnPd ₃	WIr ₃	IrW ₃	VPt ₃	ZrPd ₃
PdAu ₃	RhMn ₃	OsCr ₃	MoNi ₃		IrZr ₃		
PtAu ₃	NbRh ₃	PtCr ₃	NbNi ₃		VMn ₃		
CoPt ₃	PtNi ₃	RhCr ₃			MoTc ₃		
CrIr ₃	ScPd ₃	RuCr ₃			OsTa ₃		
CrPt ₃	YPd ₃	IrMo ₃			PdTa ₃		
FeNi ₃	ScPt ₃	IrNb ₃			PtTa ₃		
FePd ₃	TiPt ₃	IrTi ₃					
PtFe ₃	YPt ₃	IrV ₃					
FePt ₃	ScRh ₃	OsMo ₃					
HfIr ₃	TaRh ₃	OsNb ₃					
HfRh ₃	TiRh ₃	PtNb ₃					
IrMn ₃	VRh ₃	RhNb ₃					
TaIr ₃	ZrRh ₃	NiV ₃					
TiIr ₃	PdCu ₃	PdV ₃					
VIr ₃	PtCu ₃	PtTi ₃					
ZrIr ₃	LaPt ₃	PtV ₃					
AuCu ₃		RhV ₃					
		ReMo ₃					
		ReW ₃					

boundaries between regions.

Consider the NM map. The σ -CrFe structure occurs at a wide range of compositions for different pairs of elements—it is represented on all three structural maps—and it often occurs over a wide composition range for a given pair of constituents.²⁷ This tendency is considered to be characteristic of an alloy rather than a well-ordered compound, and is thus expected to involve only a small electronegativity difference, as is seen to be the case. The structures other than this and AuCu-I involve substantially larger $\Delta\phi$. Among the systems represented, AuCu-I and AuCd are polytypically related structures² involving close-packed layers stacked in different order, while the γ -CuTi phase has a superstructure based on the CsCl. Inspection of the map shows these structurally related pairs lying adjacent to one another. With perhaps the exception of the “region” attributed to the BCr structure (the filled-in squares), the map can be divided into rather well-defined areas with few compounds falling badly out of position. The electronegativity difference and the electron vacancy count are, in combination, responsible for the success.

The sign of $\Delta\phi$ is seen to be important in the NM_2 map with the σ -CrFe and a few of the Laves structured compounds straddling the zero. No

region has been attributed to the $CuAl_2$ structure, which is represented by only six compounds here. This structure is normally sorted out by considerations involving the relative size²⁸ of the constituents from the $MoSi_2$ and $NiTi_2$ structures, which it overlaps on the map. The $MoSi_2$ structure is seen to be concentrated in two regions of differing electron vacancy count, and of $\Delta\phi$ of differing sign. Similarly, the Cu_2Mg Laves phase falls in two regions to either side of $MgZn_2$ to which it is structurally related, though in this case $\Delta\phi$ tends to stay negative. A number of compounds form in both the $MgZn_2$ and Cu_2Mg structures, and these are concentrated on the two boundaries. Johannes *et al.*²⁹ have discussed the origin of this behavior of the Laves phase. They made band-theory estimates of the relative energies of the three Laves structures, with the energy of any given structure being approximated by $\int^{\epsilon_F} \epsilon \rho(\epsilon) d\epsilon$. The result was that the energy of the $MgZn_2$ structure was stable, relative to that of $MgCu_2$, for the two observed regions of electron count.

Only three structures are represented in substantial numbers in the NM_3 maps. Four structures, $CuTi_3$, $TiAl_3$, $SnNi_3$, and $TiNi_3$ involve six or fewer examples. These four are structurally related to $AuCu_3$. $CuTi_3$ and $TiAl_2$ involve² te-

tragonal distortions of the AuCu_3 structure, and lie within a common ellipse. AuCu_3 , TiNi_3 , and SnNi_3 are structural polytypes² involving different stacking of crystal layers. The latter two fall in separate small ellipses within the AuCu_3 region. A substantial overlap is seen among NM_3 compounds forming in the σ -CrFe and the related³⁰ A-15 structures. What is more, many of the pairs of constituents forming in the A-15 structure also form in the σ phase at a different composition corresponding to a slightly smaller electron vacancy count, i.e., slightly to the right on the map. The overlap region is thus associated with a tendency for both structures to occur.

It is not our purpose in displaying these maps (Fig. 3) to claim that the band-theory-based electronegativity scale is numerically superior to other scales. In fact, employing either of the other two electronegativity scales represented in Fig. 1 would yield qualitatively similar maps. Conversely, in preliminary attempts to apply our scale to Miedema's scheme to predict heats of formation, we find that the results are not substantially poorer than using the Miedema ϕ^* . This follows because, with a few exceptions such as Ru, the two scales are very much alike.

Replacing the average electron vacancy count \bar{N}_v by the electron-to-atom ratio \bar{N}_e [see Eq. (6)] has some modest effect. On the whole, N_v and N_e for the individual elements track each other rather faithfully, but the change in N_v on going from Ni, Pd, and Pt to Cu, Ag, and Au is $\sim \frac{1}{2}$, whereas it is 1.0 on the N_e scale. This does effect the resolution of the BCr, γ -CuTi, and AuCd structures on the NM map, with \bar{N}_e doing the poorer job. Our particular choice of parameters for the maps has the virtue of having been based on a common band-theory description of the transition metals.

VI. CONCLUSION

One purpose of this paper has been to consider structural maps for transition-metal compounds employing parameters derivable from band theory. In all three maps, structurally related phases tend to fall in adjacent regions. The same tendency was seen previously⁹ for compound formation between transition and nontransition elements. The relative size of the constituent atoms is not explicitly accounted for in the parameters used in the maps despite the fact that relative size is often important to the structure in which a compound forms. Nonetheless, the maps are quite successful, with the possible exception of resolving CuAl_2 from the MoSi_2 and NiTi_2 structures—a case where size considerations do seem to predominate.

Charge flow in d -electron count changes depends, of course, on the relative concentrations of constituents as well as on the magnitude of $\Delta\phi$. Granted charge conservation, charging effects are more severe at the minority site. Having defined $\Delta\phi$ to be the minority minus the majority element ϕ , we have seen that the sign of $\Delta\phi$ is important to the success of the structural maps. The sign of $\Delta\phi$ was previously seen⁹ to be important for structural maps for compound formation between transition and nontransition elements as well. This dependence on ϕ is a subtler, higher-order effect than the quadratic dependence on $\Delta\phi$ that enters our understanding of alloy solubilities, and in Miedema's formulation of alloy heats of formation. It may be somewhat analogous to Simons and Bloch's S factor, which also is a subtler measure, in this case, of the relative propensity for s vs p electron bonding in nontransition elements. The role of such factors in a general understanding of alloy formation requires considerable further investigation.

The σ phase appears in all three maps. It involves a small electronegativity difference befitting an alloy system displaying substantial composition ranges. As has already been recognized,¹⁻³ it occurs for a narrow electron vacancy range centered on $\bar{N}_v = 4$. This phase is also of considerable practical interest: it is the phase that can cause embrittlement of high-temperature steels and superalloys. It and the phases to which it is structurally related are the object of continuing investigation.

The principal purpose of this paper has been the derivation of the new ϕ scale and the physical insights offered by deriving such a scale from the electron-band-theory properties of transition metals. As we have already suggested, there may well be no unique electronegativity scale that can be universally applied to all occasions where "electronegativity" is invoked. The present results do suggest certain tendencies, e.g., that the noble metals are less electronegative than the transition metals immediately adjacent to them. This result presumes that the noble metals can be treated on an identical basis with the transition metals. It was also seen that the heavy $3d$ elements are only moderately less electronegative than their $4d$ and $5d$ counterparts. We leave to future work the question of whether there is a complementary band-theory basis for electronegativity among the nontransition elements.

ACKNOWLEDGMENT

Research at BNL was supported by the U. S. Department of Energy under Contract No. EY-76-C-02-0016.

- ¹C. S. Barrett and T. B. Massalski, *Structure of Metals* (McGraw-Hill, New York, 1979).
- ²W. B. Pearson, *The Crystal Chemistry and Physics of Metals and Alloys* (Wiley, New York, 1972).
- ³W. Hume-Rothery, *Elements of Structural Metallurgy* (Institute of Metals, London, 1961).
- ⁴E. A. Stern, *Phys. Rev. B* **7**, 1303 (1973).
- ⁵J. T. Waber, K. Gschneidner, Jr., A. C. Larson, and M. Y. Prince, *Trans. Metall. Soc. AIME* **227**, 717 (1963).
- ⁶A. R. Miedema, *J. Less Common Met.* **46**, 67 (1976); A. R. Miedema, F. R. de Boer, and R. Boom, *Calphad* **1**, 341 (1977), and references therein.
- ⁷R. S. Mulliken, *J. Chem. Phys.* **46**, 497 (1949); H. A. Skinner and H. O. Prichard, *Trans. Faraday Soc.* **49**, 1254 (1953).
- ⁸G. Simons and A. N. Bloch, *Phys. Rev. B* **7**, 2754 (1973); A. N. Bloch and G. Simons, *J. Am. Chem. Soc.* **94**, 8611 (1972); J. St. John and A. N. Bloch, *Phys. Rev. Lett.* **33**, 1095 (1974).
- ⁹R. E. Watson and L. H. Bennett, *J. Phys. Chem. Solids* **39**, 1235 (1978).
- ¹⁰W. Gordy and W. J. O. Thomas, *J. Chem. Phys.* **24**, 439 (1956).
- ¹¹L. Pauling, *Nature of the Chemical Bond*, 3rd ed. (Cornell University, Ithaca, 1960).
- ¹²P. H. Barrett, R. W. Grant, M. Kaplan, D. A. Keller, and D. A. Shirley, *J. Chem. Phys.* **39**, 1035 (1963).
- ¹³R. M. Friedman, J. Hudis, M. L. Perlman, and R. E. Watson, *Phys. Rev. B* **8**, 2433 (1973); C. D. Gelatt, Jr., and H. Ehrenreich, *Phys. Rev. B* **10**, 398 (1974).
- ¹⁴R. E. Watson and L. H. Bennett, *Phys. Rev. B* **15**, 5136 (1977); **17**, 3714 (1978); *Hyperfine Interactions* **4**, 806 (1978).
- ¹⁵E. S. Machlin, T. P. Chow, and J. C. Phillips, *Phys. Rev. Lett.* **38**, 1292 (1977).
- ¹⁶J. R. Chelikowsky and J. C. Phillips, *Phys. Rev. Lett.* **39**, 1687 (1977); *Phys. Rev. B* **17**, 2453 (1978).
- ¹⁷Clearly there is a hybridization energy associated with Eq. (2). It is of significance, but will not be considered here.
- ¹⁸(Au) N. E. Christensen and B. O. Seraphin, *Phys. Rev. B* **1**, 1443 (1970); (Re) L. F. Mattheiss, *Phys. Rev.* **151**, 450 (1966); (Zr and Hf) O. Jepsen, O. K. Andersen, and A. R. Mackintosh, *Phys. Rev. B* **12**, 3084 (1975). (Nb and Ta), L. F. Mattheiss, *ibid.* **1**, 373 (1970); (Fe) L. F. Mattheiss, *Phys. Rev.* **139**, 206 (1965).
- ¹⁹V. Heine, *Phys. Rev.* **153**, 673 (1967).
- ²⁰L. Hodges, R. E. Watson, and H. Ehrenreich, *Phys. Rev. B* **5**, 3953 (1972).
- ²¹T. S. Chou, M. L. Perlman, and R. E. Watson, *Phys. Rev. B* **14**, 3248 (1976).
- ²²Au-Pt may offer the exception. Analysis (see Ref. 21) indicates charge transfer onto the Au site, but the transfer is small in magnitude and charge transfer of opposite sign, i.e., off Au, lies within the error bar of the analysis.
- ²³E. C. Stoner, *Rep. Prog. Phys.* **11**, 43 (1946/47).
- ²⁴Note, however, that the *s-d* one-electron energy separations are important to the band-theory electronegativity results. The *d* levels are low with respect to the continuum for the heavy *4d* metals, causing the *N* of Table I to be small relative to their *3d* and *5d* counterparts. This tends to increase the ϕ of Rh and Pd. The same energy trend causes the Ag *4d* bands to lie well below ϵ_F , reducing its ϕ value.
- ²⁵A similar situation is encountered in Miedema's formulation of heats of formation, where the electronegativity and the electron density are employed as "independent" parameters. The two quantities are intimately related, yet provide a most successful basis for predicting heats of formation.
- ²⁶For this reason, the electron vacancies are mostly plotted in Fig. 3 for the median instead of the stoichiometric composition for the σ phases.
- ²⁷Landolt-Börnstein New Series Vol. 6, *Structure Data of Elements and Intermetallic Phases*, edited by K.-H. Hellwege and A. M. Hellwege (Springer-Verlag, Heidelberg, 1971).
- ²⁸M. V. Nevitt, in *Intermetallic Compounds*, edited by J. H. Westbrook (Wiley, New York, 1967), p. 217.
- ²⁹R. L. Johannes, R. Haydock, and V. Heine, *Phys. Rev. Lett.* **36**, 372 (1976).
- ³⁰C. B. Shoemaker and D. P. Shoemaker, in *Developments in the Structural Chemistry of Alloy Phases*, edited by B. C. Giessen (Plenum, New York, 1969), p. 107.